Cell

Resource

High-Content siRNA Screen Reveals Global ENaC Regulators and Potential Cystic Fibrosis Therapy Targets

Joana Almaça,[1,5] Diana Faria,[1,2,5] Marisa Sousa,[1] Inna Uliyakina,[1] Christian Conrad,[3] Lalida Sirianant,[2] Luka A. Clarke,[1] José Paulo Martins,[4] Miguel Santos,[4] Jean-Karim Heriché,[3] Wolfgang Huber,[3] Rainer Schreiber,[2] Rainer Pepperkok,[3] Karl Kunzelmann,[2] and Margarida D. Amaral[1,*]

[1]University of Lisboa, Faculty of Sciences, BioFIG - Centre for Biodiversity, Functional and Integrative Genomics, Campo Grande, C8 bdg, 1749-016 Lisboa, Portugal

[2]Department of Physiology, University of Regensburg, 93053 Regensburg, Germany

[3]Cell Biology/Biophysics Unit, European Molecular Biology Laboratory (EMBL), 69117 Heidelberg, Germany

[4]EcBio - R&D in Biotechnology SA, 2700-451 Amadora, Portugal

[5]These authors contributed equally to this work

*Correspondence: mdamaral@fc.ul.pt

http://dx.doi.org/10.1016/j.cell.2013.08.045

SUMMARY

Dysfunction of ENaC, the epithelial sodium channel that regulates salt and water reabsorption in epithelia, causes several human diseases, including cystic fibrosis (CF). To develop a global understanding of molecular regulators of ENaC traffic/function and to identify of candidate CF drug targets, we performed a large-scale screen combining high-content live-cell microscopy and siRNAs in human airway epithelial cells. Screening over 6,000 genes identified over 1,500 candidates, evenly divided between channel inhibitors and activators. Genes in the phosphatidylinositol pathway were enriched on the primary candidate list, and these, along with other ENaC activators, were examined further with secondary siRNA validation. Subsequent detailed investigation revealed ciliary neurotrophic factor receptor (CNTFR) as an ENaC modulator and showed that inhibition of (diacylglycerol kinase, iota) DGKι, a protein involved in PiP2 metabolism, downgrades ENaC activity, leading to normalization of both Na^+ and fluid absorption in CF airways to non-CF levels in primary human lung cells from CF patients.

INTRODUCTION

ENaC, the epithelial sodium (Na^+) channel is a major player in salt and water reabsorption and epithelial surface hydration in a number of tissues, including airways and alveolar sacs, ducts of exocrine glands, renal collecting duct, and distal colon. ENaC plays a prominent role in lung liquid clearance by the alveolar epithelium after birth by reabsorbing fetal lung fluid (O'Brodovich, 1991).

As a member of the degenerin ion channel family, ENaC consists of three main subunits, α-, β- and γ-ENaC (Canessa et al., 1994). ENaC impairment leads to diverse diseases with the hallmark of local or systemic imbalance in Na^+ and water homeostasis. ENaC loss-of-function results for example in renal salt wasting (type I pseudohypoaldosteronism) or pulmonary edema (Berthiaume and Matthay, 2007). In contrast, ENaC gain-of-function leads to several forms of salt-sensitive hypertension (e.g., Liddle syndrome) or cystic fibrosis (CF) (Bonny and Hummler, 2000; Lifton et al., 2001; Donaldson and Boucher, 2007).

CF is a life-threatening disease caused by mutations in the gene encoding the CF transmembrane conductance regulator (CFTR) protein, a chloride (Cl^-) channel localized in the apical membrane of epithelial cells (Riordan, 2008). Physiologically, CFTR inhibits ENaC and thus regulates pulmonary Na^+ absorption (Kunzelmann et al., 1995; Gentzsch et al., 2010). In CF, however, the absence of active CFTR leads to Na^+ hyperabsorption, which causes dehydration of airway surface liquid (ASL), a hallmark of CF (Boucher, 2007; Mall et al., 1998). Compelling evidence for the major role that ENaC plays in CF airways came from βENaC-overexpressing mice, which mimic various aspects of human CF respiratory disease (Mall et al., 2004). This is in striking contrast to CFTR knockout or CFTR mutant mice, which do not develop lung disease (Snouwaert et al., 1992).

Membrane levels of ENaC are mostly regulated by endocytosis and proteolysis mediated by the E3-ubiquitin-ligase Nedd4-2. Another mouse model, a lung-specific Nedd4-2 knockout, was shown to also develop a CF-like condition (Kimura et al., 2011), further establishing the key role of ENaC in CF airway disease.

So, along with the search for small molecules to restore CFTR activity, ENaC inhibitors have been sought for CF therapeutics to reduce ENaC-mediated Na^+ hyperabsorption and increase ASL hydration (Amaral and Kunzelmann, 2007). Such a goal might also be of interest to treat chronic obstructive lung disease (COPD), disseminated bronchiectasis, or even CFTR dysfunction caused by cigarette smoking (Clunes et al., 2012). ENaC

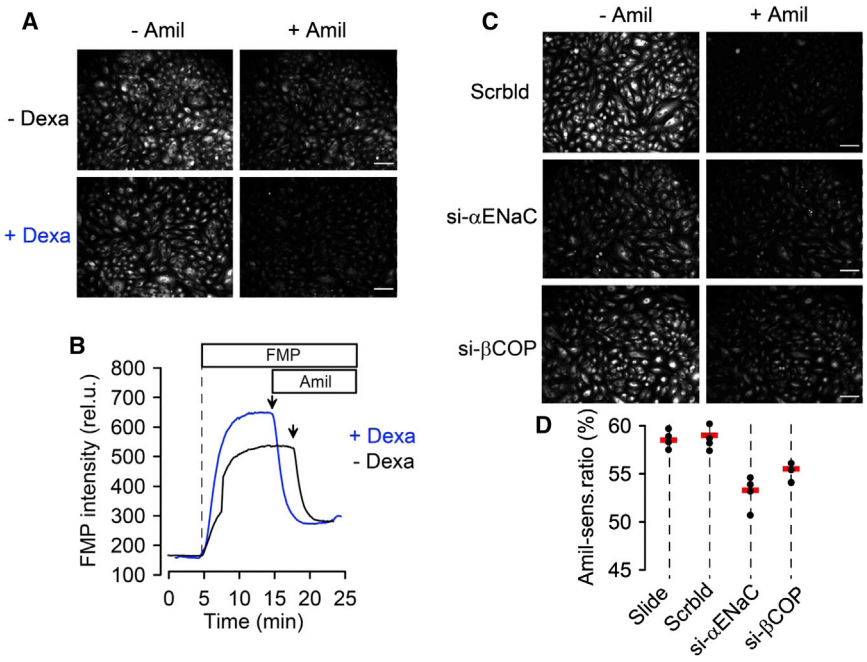

Figure 1. ENaC Functional Screening Assay

(A) Images of A549 cells subjected to the FMP/Amil assays before (left) and after Amil (right). Cells grown for 48 hr under dexamethasone (+Dexa, top) demonstrated enhanced FMP/Amil quenching (higher ENaC activity) than cells grown in the absence of Dexa (bottom).

(B) Quantification of the Amil-sensitive FMP fluorescence of images in A shows greater ENaC activity in cells grown under Dexa.

(C) Images of A549 cells grown for 48 hr under Scrbld, αENaC, or ßCOP siRNAs.

(D) Summary of the median ratio Amil-sensitive FMP fluorescence ratios for all spots in the same slide ("slide"), scrambled ("Scrbld"), αENaC and ßCOP siRNA spots. Average of Amil-sensitive ratios (n = 5) is shown as a red line ± SD.

blockers may also serve to hydrate mucosal surfaces of the gastrointestinal tract, mouth, nose, and eye and treat ENaC gain-of-function conditions, like ENaC-related hypertension (Butterworth et al., 2009). Amiloride (Amil), used for the management of hypertension and congestive heart failure, was the first ENaC pharmacological inhibitor tested in CF, but studies showed no significant improvement due to its short half-life in the lungs (Knowles et al., 1990). Longer-acting and more potent ENaC inhibitors (IC_{50} ~10 nM) include Amil derivatives such as benzamil or PS552 (Parion Sciences, Durham, NC), both yielding disappointing results in CF trials (Donaldson and Boucher, 2007; Hirsh et al., 2006). Excessive blocking of ENaC may cause severe harm, via undesirable accumulation of fluid in the lungs, i.e., pulmonary edema (Althaus et al., 2011). Instead, we need compounds normalizing ASL homeostasis through physiological regulation of ENaC. If achieved independently of CFTR, such normalization could correct ion transport in CF patients with any CFTR mutation.

Despite detailed knowledge on how several ENaC regulators control both channel number at the cell surface and its open probability (Butterworth et al., 2009), many aspects of ENaC biogenesis, trafficking, and regulation remain obscure. Herein, we have undertaken a large-scale loss-of-function (siRNA) screen for ENaC with the ultimate goal of identifying putative druggable targets. We used a live-cell assay and automatic microscopy to functionally assess ENaC in human respiratory epithelial cells after reverse siRNA transfection (Erfle et al., 2007) with libraries targeting a total of 6,396 genes. We thus identified 1,626 genes regulating ENaC: 887 inhibitors and 739 activators. Bioinformatic analyses of primary hits identified the phosphatidylinositol (PI) pathway as the top enriched pathway (with 30 hits), 37% of which were validated. The top ~60% primary ENaC-hits also underwent reassessment, achieving ~30% validation.

The validated hits were then classified into known ENaC regulatory pathways. Seven genes were found to lie outside such pathways and 2 of these were chosen for further investigation and shown to be key ENaC regulators: diacylglycerol kinase iota (*DGKι*), a potential robust CF therapeutic target; and ciliary neurotrophic factor receptor (*CNTFR*), an original ENaC modulator, which proved the screen's power to identify novel hits.

RESULTS

Live-Cell siRNA Screen Identifies 1,626 ENaC Regulators

For the high-content siRNA screen, we used a live-cell assay measuring ENaC activity through the voltage-sensitive fluorescent FMP dye in combination with specific ENaC blocker Amil (Almaça et al., 2011). Human alveolar epithelial cells A549 (with endogenous ENaC expression) were grown under dexamethasone (Dexa) to maximize ENaC expression (Figures 1A and 1B) (Itani et al., 2002). Cells were transfected with siRNAs targeting α-ENaC subunit or ßCOP (component of traffic vesicles) as positive controls and scrambled siRNA (Scrbld) as negative control. As expected both α-ENaC and ßCOP siRNAs (but not Scrbld) significantly suppressed the quenching of Amil-induced fluorescence (Figures 1C and 1D). The difference between the values for positive (si-αENaC/ si-ßCOP) and Scrbld or "slide score" (see Supplemental Information) is relatively modest (~10%). However, due to high reproducibility and lack of overlap between positive and negative controls (Figure 1D) we could proceed to high-content microscopy screening. Indeed, the robustness of the microscopy approach and image analysis, allowing collection of cell-based multi-information data (number of cells, removal of debris, apoptotic cells, etc.), enabled quality control, which, together with "local background" correction and robust statistics (Chung et al., 2008) led to reliable and reproducible hit discrimination.

For the automated high-throughput microscopy screen, we individually silenced 6,396 protein-coding human genes, using

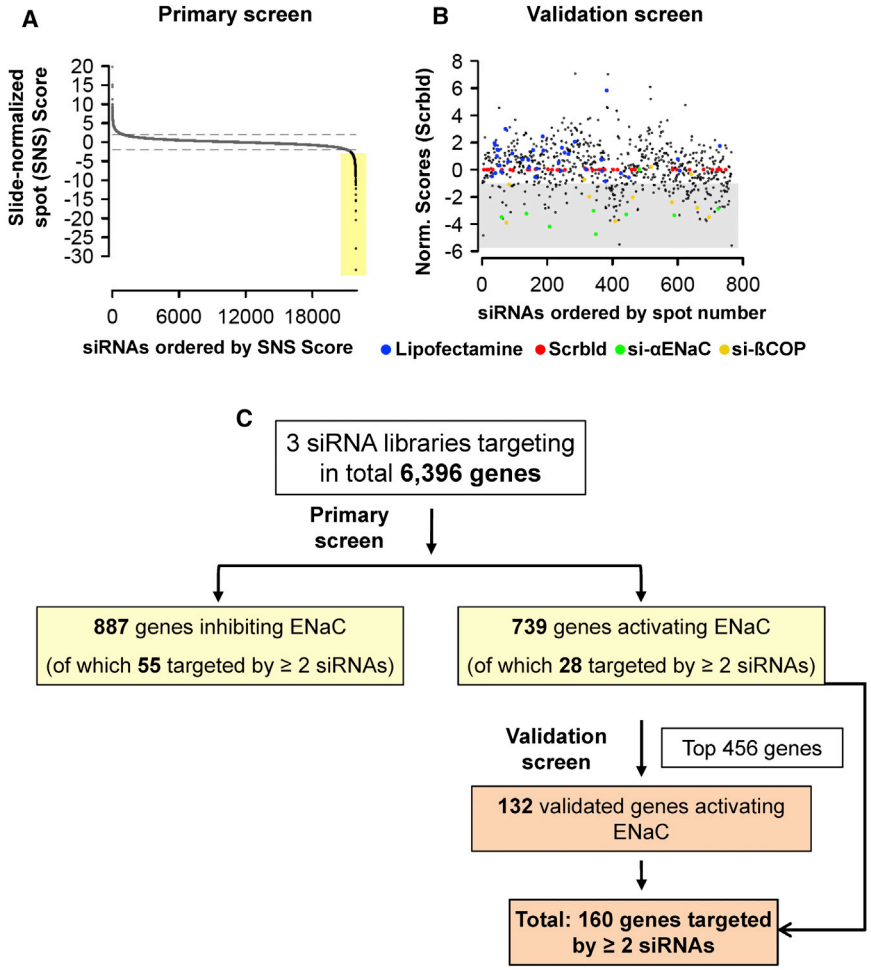

Figure 2. Overview of Screen Data

(A) Distribution of averaged "SNS-score" values obtained for every siRNA in the primary screen. The "SNS-scores" calculated for each siRNA spot and averaged among replicates were used to assess how each siRNA affected ENaC activity. siRNAs with SNS-scores ≥ 2 or ≤ -2 (black dashed horizontal lines) were considered as ENaC activators or inhibitors (yellow shade) siRNAs, respectively. See also Figures S1 and S2 and Datasets S1 and S2.

(B) Scatter plot of data from the validation screen where each siRNA is represented as the average of "spot scores": blue,"empty spots" (i.e., lipofectamine with no siRNA); red, Scrbld; green, si-αENaC; orange, si-ßCOP. The threshold used (red line) was the minimum normalized score among "empty spots." See also Dataset S3 and Figures S3.

(C) Workflow showing the different steps in the primary and validation screens and the number of hit genes after each step.

2-3 siRNAs per gene (n = 17,622) and monitored their effects on ENaC activity by the FMP/Amil assay. The result for each siRNA consisted in the "slide-normalized spot score" ("SNS-score") averaged from siRNA replicates (Dataset S1A available online). SNS-scores were put into an ordered distribution (Figure 2A) and siRNAs with SNS-scores ≤ -2 were considered as inhibiting ENaC (Dataset S1B), whereas those with SNS-scores ≥ 2 were considered as activating ENaC (Dataset S1C, Figure 2A). In summary (Figure 2C), this primary screen revealed 1,626 hits: 739 genes activating ENaC, i. e., targeted by siRNAs inhibiting ENaC (highlighted in yellow in Figure 2C): 711 with one, 27 with two and 1 with 3 siRNAs plus 887 genes inhibiting ENaC, i.e., targeted by ENaC-activating siRNAs: 832 with one, 52 with two and 3 with three siRNAs. All 1,626 ENaC regulator hits were analyzed by DAVID bioinformatic tool for functional annotation, which revealed the phosphatidylinositol (PI) pathway (KEGG hsa04070) as the most significantly enriched with 30 genes, $p < 2x10^{-6}$ (Dataset S2 and Figure S1). After validation by stringent selection criteria 11 (37%) of these 30 genes could be established as "truly confirmed" hits with two or more siRNAs (Dataset S3A and Figure S1): 10 ENaC activators (*CDS1*, *DGKA*, *DGKI*, *ITPK1*, *ITPR3*, *PIK3CB*, *PIK3CD*, *PIP4K2A*, *PLCB1*, *PLCZ1*) and 1 ENaC inhibitor (*PIK3C2B*). Although other genes among the 30 had at least two siRNAs that confirmed the primary screen, they also had another siRNA with opposite effect and thus they were not considered as hits.

As we aimed to identify ENaC activators (to be inhibited by small molecules), we also sought for additional siRNA validation of the top 60% ENaC-activating genes (456 out of 739 activator genes). The normalized results of this validation screen are displayed as a scatter plot in Figure 2B and siRNAs below the -1 threshold were considered as hits (gray area, Figure 2B). This is the minimum normalized score for "empty spots" (i.e., positions with lipofectamine only, no siRNA). We thus confirmed 132 (~30%) out of the rescreened 456 primary screen hits (Figure 2C). These, together with hits targeted by at least two siRNAs in the primary screen, identified 160 ENaC-activator genes (Figure 2C, Dataset S3B). As most of these hits encode proteins never reported as ENaC regulators, we used Gene Ontology (GO) terms to classify them (Figure S2). We also checked their role in previous screens using the same siRNAs or in other relevant studies (Dataset S3B). Interestingly, the largest group (33%) had been previously implicated in secretory trafficking (Simpson et al., 2012), followed by 23% in cell division (Neumann et al., 2010), 5% in plasma membrane targeting of Src kinases (Ritzerfeld et al., 2011), and 3% in a global set of CFTR interactors (Wang et al., 2006). Notably, in the latter group we found *CFTR* itself (plus *APC*, *RYK*, *HSP90B1*, *COPB1*).

Experimental Hit Classification into Known ENaC Pathways and Further Bioinformatic Analyses

To gain mechanistic insight into how the validated hits regulate ENaC, we performed the same FMP/Amil assay for these genes

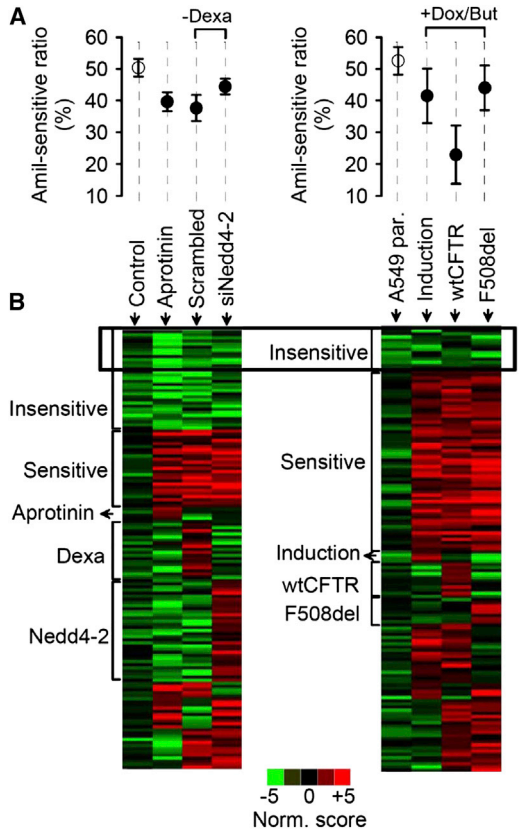

Figure 3. ENaC Pathway Classification of Validated Hits

(A) Validated hits were experimentally classified into known ENaC-regulating pathways by the same FMP/Amil assay after various treatments (see text). Graph shows mean values of % Amil-sensitive ratio ± SD (n = 16 spots).

(B) Heat maps showing normalized scores for siRNAs targeting the validated hits and their sensitivity to various treatments, as indicated. Score values range from −5 (green, inhibitory siRNA) to +5 (red, activatory siRNA).

See also Figure S4 and Datasets S4 and S5.

under conditions that interfere with pathways known to affect ENaC, namely: (1*)* incubation of cells with protease inhibitor aprotinin to inhibit ENaC activation by proteolytic cleavage (Gaillard et al., 2010) by; (2*)* under Nedd4-2 siRNA transfection to inhibit ENaC endocytosis mediated by the Nedd4-2/SGK1 pathway (Staub et al., 1997; Debonneville et al., 2001); and (3*)* after induction of WT- (or F508del-) CFTR expression in transduced A549 cells to inhibit (or not) ENaC (Kunzelmann et al., 1995; Almaça et al., 2011).

Data in Figure 3A (left graph) show first that aprotinin-treated cells exhibit a modest but consistent and significant decrease (∼20%) in the Amil-sensitive ratio versus control cells, as expected due to inhibition of ENaC activation by serine endopeptidases. Second, data show (Figure 3A, left) that removal of Dexa (6h) already causes significant ENaC inhibition, which, however, can be reverted by Nedd4-2 siRNA with a significant ∼15% increase versus control cells. Third, induction of WT-CFTR expression (but not of F508del-CFTR) by doxycycline and butyrate (Dox/but), causes a significant decrease in ENaC function of ∼50% (Figure 3A, right graph). By recapitulating the in vivo regulation of ENaC by CFTR (Kunzelmann et al., 1995), these cells are thus very useful to test how the novel ENaC regulators relate to CFTR.

Next, by rescreening the validated ENaC activators under these 3 conditions we classified them according to such pathways (heat-maps in Figure 3B). For example, under Nedd4-2 downregulation, ∼56% of the siRNA hits no longer inhibited ENaC (“Nedd4-2-sensitive” hits) suggesting that they exert their effects on this pathway and indicating the central role that this E3-ubiquitin ligase plays on ENaC regulation. Also, in the presence of aprotinin, ∼32% of the siRNA hits no longer inhibited ENaC, suggesting that their effects on ENaC are protease-mediated.

Based on their sensitivity to these treatments, the validated hits were grouped into 5 different classes (Figure 3B and Dataset S4): (1) class I (∼23%) insensitive to all treatments; (2) class II (∼18%) sensitive to all three treatments; (3) class III, (4) class IV, (5) class V, hits sensitive only to aprotinin (∼3%), 6h-Dexa (∼13%) or Nedd4-2-siRNA (∼23%), respectively. Additional sets (classes VI, VII and VIII) include hits that are sensitive to two out of the three treatments (Dataset S4). Classification of hits according to their CFTR-dependence produced additional classes (marked “*,”Dataset S4). For example, class IV* includes hits no longer affecting ENaC upon WT-CFTR expression. Of particularly interest are hits showing differential effects in the presence of WT- versus F508del-CFTR (classes IV* and V*) as they may be key to elucidate how WT-CFTR (but not F508del-CFTR) prevents ENaC-mediated Na^+ hyperabsorption in non-CF individuals. Seven hits were insensitive to all treatments (classes “I and I*”) namely: *ACY3*; *CCNI*; *CNTFR*; *DGKι*; *IQCF1*; *MEST*; *SERPINB3*. As they fall out of known ENaC regulatory pathways they deserve further investigation.

To select for putative drug targets and learn more about the validated genes, additional bioinformatic analyses were performed, including a measure of their “closeness to ENaC,” given by “cosine similarity” values (see Supplemental Information). This was based on the proteases-Nedd4-2 scores (Dataset S4B) and used as reference values for si-αENaC: the higher the cosine similarity the closer genes are to ENaC (Dataset S5 and Figure S3). We also submitted the above 7 “insensitive” hits to predictive protein-protein functional correlations (FunL, see Supplemental Information) in relation to ENaC. From the resulting network (Figure S4) two genes emerged functionally closer to ENaC: *CNTFR* and *DGKι*. We next selected both genes for further studies.

Although DGK was a recognized ENaC regulator (Kunzelmann et al., 2005), its DGKι isoform was mechanistically evaluated here as a possible drug target for CF. Indeed, four main reasons led to selection of DGKι: first, DGKι emerged as a key hit in the top-enriched pathway—the PI signaling system (Figure S1 and Dataset S2); second, the DGKι isoform was found to be highly expressed in human airways (Figure S5); third, bioinformatic analysis (Figure S3) ranked DGKι very close to ENaC (nr.11) even higher than CFTR (nr.14); finally, as a kinase, it is amenable to small-molecule inhibition and thus a good drug target. CNTFR in turn, was also further investigated as an original hit due to its bioinformatic proximity to ENaC (Figures S3 and S4) and to demonstrate the screen’s power to identify original hits.

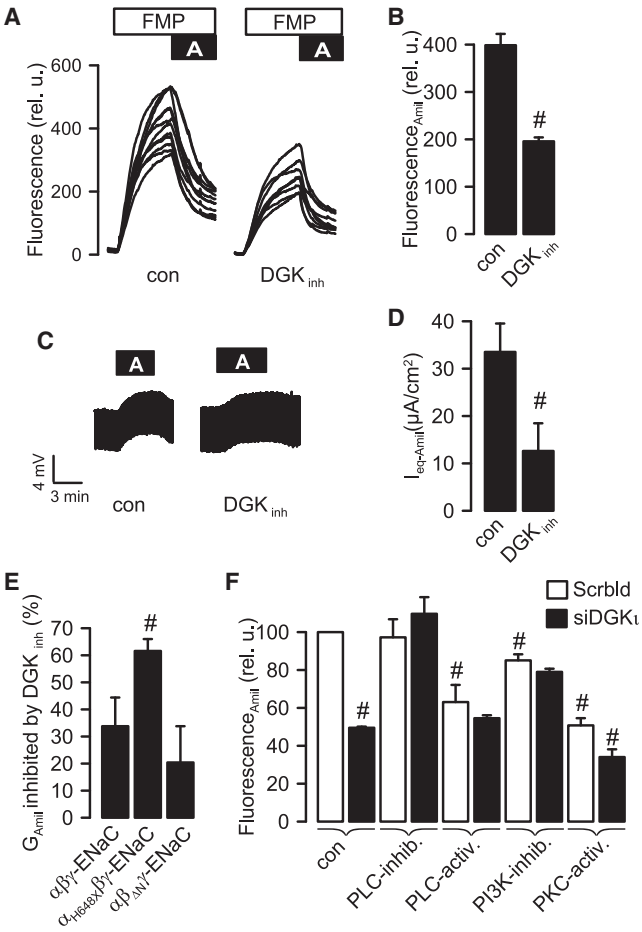

Figure 4. Regulation of ENaC by DGK

(A) Recordings of voltage-dependent FMP fluorescence in individual A549 cells demonstrate fluorescence decrease after application of Amil, due to hyperpolarization of the membrane voltage.

(B) Summary of data shows inhibition of Amil-induced quenching in A549 cells after inhibition of DGK (DGK_{inh}, 25 μM).

(C) Original Ussing chamber recordings of transepithelial voltages (V_{te}) assessed in mouse trachea before and after treatment with DGK_{inh} (25 μM, 1-2 h; n = 13).

(D) Summary of $I_{eq\text{-}Amil}$ in mouse trachea demonstrating inhibition of ENaC by DGK_{inh}.

(E) Summary of the effects of DGK_{inh} on ENaC activity measured as Amil-sensitive conductances (G_{Amil}) in *Xenopus* oocytes expressing WT-αβγENaC, truncated $\alpha_{H648X}\beta\gamma$ENaC, or $\alpha\beta_{\Delta N}\gamma$-ENaC lacking an N-terminal PIP_2-interaction domain in β-subunit ($\alpha\beta_{\Delta N}\gamma$-ENaC) (each n = 12).

(F) FMP assay on A549 cells treated with either with Scrbld or si-DGKι-siRNA. Cells were incubated for 2–5 hr with compounds inhibiting PLC (U73122; 20 μM) or activating PLC (m3M3FBS; 25 μM), inhibiting PI3K (LY294002; 10 μM) or activating PKC (PMA; 10 μM).

Mean ± SEM. #, significant difference versus controls (unpaired t test and ANOVA; $p < 0.05$). See also Figure S5.

DGKι: a Robust Therapeutic Target for ENaC

DGKι was thus investigated as a drug target candidate for ENaC regulation and results in various cell types showed that it is essential for maintenance of ENaC activity. First, we showed that a chemical blocker of DGK (DGK_{inh}, 25 μM) led to ~50% ENaC inhibition in A549 cells (Figures 4A and 4B). Second, in mouse tracheas assessed ex vivo in Ussing chambers, DGK_{inh} attenuated Amil-induced voltage deflection and inhibited Amil-sensitive short-circuit current, indicating inhibition of ENaC by ~60% (Figures 4C and 4D). Third, these data were confirmed in polarized H441 human airway epithelial cells and M1 mouse collecting duct cells (data not shown), as well as after coexpression of three ENaC subunits (αβγ) in *Xenopus* oocytes, where the Amil-inhibited whole-cell conductance (G_{Amil}) was ~30% inhibited by DGK_{inh} (Figure 4E, left bar).

To better understand the underlying mechanisms, we assessed ENaC conductance in *Xenopus* oocytes, by coexpressing DGKι and WT- or truncated (α_{H648X}) αENaC with WT-βγENaC. We found that ~60% of G_{Amil} produced by α_{H648X} βγENaC was inhibited by DGK_{inh}, in contrast to only ~30% for αβγENaC (Figure 4E). The truncated α_{H648X} lacks an essential binding site for the ubiquitin ligase Nedd4-2, resulting in enhanced ENaC-activity (G_{Amil} = 107.27 ± 26.4 versus 47.25 ± 4.8 μS) that is fully subjected to regulation by PIP_2 and DGK_{inh} (Yue et al., 2002; Kunzelmann et al., 2005). The inhibitory effect of DGKι-siRNA on ENaC was therefore augmented because-Nedd4-2-dependent regulation is largely reduced for α_{H648X} βγENaC. In contrast, deletion of the N terminus of β-ENaC largely inhibited ENaC conductance (G_{Amil} = 1.4 ± 0.5 μS) and only ~20% of the remaining conductance was inhibited by DGK_{inh} (Figure 4E, right bar). Because binding of N terminus of β-ENaC to PIP_2 is essential to maintain ENaC activity (Pochynyuk et al., 2007), these data support the concept that DGK activates ENaC by maintaining sufficiently high PIP_2 levels.

This conclusion was further substantiated by pharmacological manipulation of enzymes that are crucial for PI metabolism and ENaC activity, some of which were hits in the primary screen (Figure S1). Using Amil-sensitive FMP fluorescence in A549 cells as a measure for ENaC activity, siRNA-DGKι was confirmed to inhibit by ~50% ENaC activity, whereas Scrbld had no effect (Figure 4F, black versus white bars, respectively). Inhibition of phospholipase C (PLC) by its blocker U73122, which antagonizes hydrolysis of PIP_2, completely abrogated the inhibitory effects of siRNA-DGKι on ENaC (Figure 4F). In contrast, stimulation of PLC by its activator m3M3FBS inhibited ENaC by ~40% and importantly, abolished further inhibition of ENaC by siRNA-DGKι. These results clearly indicate that DGKι activates ENaC by maintaining the PIP_2 pool in the inner membrane leaflet. The PiP_2 content may also be lowered by phosphatidylinositol-4,5-biphosphate 3-kinase (PI3K) that converts PIP_2 into PIP_3 - phosphatidylinositol (3,4,5)-trisphosphate (Figure S1). Accordingly, inhibition of PI3K by its inhibitor LY294002 slightly reduced ENaC activity because PIP_3 is a positive ENaC regulator (Pochynyuk et al., 2007). Notably however, in the presence of the PI3K inhibitor, siRNA-DGKι no longer inhibited ENaC (Figure 4F), plausibly because of enhanced PIP_2 pools. However, PI3K itself is not a specific target to control ENaC activity because, in contrast to DGK that is confined to the resynthesis of apical PIP_2, PI3K controls numerous cellular processes (reviewed in Pochynyuk et al., 2008). DGKι is thus an advantageous target to inhibit ENaC through PIP_2 in the airways because it localizes exclusively to the apical membrane of epithelial cells and in close proximity to ENaC, where it rather specifically controls apically located ion channels.

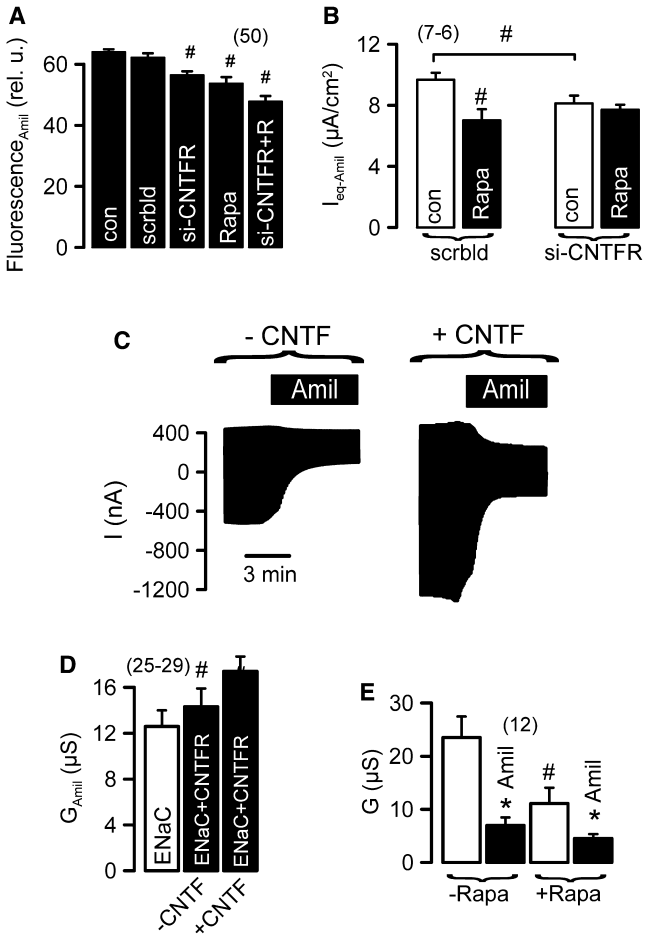

Figure 5. Regulation of ENaC by CNTFR and Effect of mTOR Inhibition by Rapamycin

(A) Summary of the effects of si-CNTFR or mTOR inhibition by rapamycin (or both together) on ENaC activity, measured by Amil-sensitive FMP fluorescence in H441 cells (n = 50 for all series).

(B) Summary of mTOR inhibition by rapamycin on Amil-sensitive $I_{eq-Amil}$ as measured in open-circuit Ussing chamber measurements of polarized grown H441 cells treated with siCNTFR or Scrbld (n = 6–7).

(C) Original recordings of whole-cell currents measured in CNTFR/ENaC co-expressing oocytes showing enhanced Amil-sensitive Na^+ currents after 24 hr incubation with CNTF (CNTFR ligand).

(D) Summary of effects of CNTF incubation on Amil-sensitive whole-cell conductances measured in ENaC-expressing *Xenopus* oocytes (n = 25–29).

(E) Effects of mTOR inhibition by rapamycin on Amil-sensitive conductance (n = 12).

Mean ± SEM. #, different to control; $p < 0.05$; ANOVA. * indicates significant inhibition by Amil; $p < 0.05$; paired t test. See also Figure S6.

Notwithstanding, inhibition of DGKι also leads to accumulation of DAG, a potent activator of protein kinase C (PKC), which is a known inhibitor of ENaC (Stockand et al., 2000). To rule out that DGKι-dependent activation of ENaC is associated with DAG-stimulated activation of PKC, we tested the effect of si-DGKι on ENaC under PKC modulation. As expected, PKC activation by phorbol 12-myristate 13-acetate (PMA) inhibited ENaC by ~50%. However, siRNA-DGKι further reduced ENaC activity, suggesting a PKC-independent inhibitory effect (Figure 4F). These results are supported by data demonstrating that the PKC-inhibitor bisindolylmaleimide (BIM) is unable to fully restore ENaC activity in si-DGKι treated cells (data not shown). Thus, DGKι activates ENaC by regenerating PIP_2 pools in the inner plasma membrane leaflet.

CNTFR: A Novel ENaC Regulator

Before further investigating CNTFR, we assessed its physiological relevance in the lung by confirming its expression in human native airways (Figure S6). Next, CNTFR expression was knocked-down by siRNA in H441 cells (as confirmed by western blot, Figure S6) and this attenuated the effects of Amil on FMP fluorescence (Figure S6C) and inhibited Amil-sensitive transport ($I_{eq-Amil}$) (Figures 5A and 5B). CNTFR couples to several intracellular pathways, one of them being the mammalian target of rapamycin (mTOR) (Yokogami et al., 2000). Thus, we next inhibited mTOR by rapamycin, which also reduced ENaC-mediated Na^+ transport (Figure 5B, left). However, rapamycin itself was without effect on $I_{eq-Amil}$ after si-CNTFR (Figure 5B, right), suggesting that CNTFR indeed acts through mTOR. CNTFR effects were further validated by its overexpression in *Xenopus* oocytes, which when coexpressed with ENaC enhanced Amil-sensitive conductance (Figures 5C and 5D). Notably, 48 hr incubation of oocytes with the cytokine CNTF (CNTFR ligand) further increased the Amil-sensitive conductance, whereas inhibition of mTOR by rapamycin strongly inhibited ENaC (Figure 5E) (Koehl et al., 2010; Ousingsawat et al., 2008). Thus, CNTF/CNTFR appears be a novel pathway regulating ENaC operating through mTOR (Lu et al., 2010). Importantly, ENaC inhibition by si-CNTFR was also confirmed in primary cultures of HBE cells from CF patients (Figure S6E).

Validation of DGKι as Drug Target for ENaC in Human CF Airways

Although the above results clearly demonstrate inhibition of ENaC by DGK_{inh}, the crucial question is whether this could be used to inhibit Na^+ hyperabsorption in CF airways. We therefore isolated airway epithelial cells from lungs of CF patients and grew them as highly differentiated polarized cultures under ALI conditions. Original Ussing chamber recordings demonstrate large Amil-induced voltage deflections, indicating pronounced ENaC activity and Na^+ absorption in CF airways (Figures 6A and 6C). ENaC in CF airways is known to be inhibited by stimulation of apical purinergic $P2Y_2$ receptors, as also shown here by pronounced attenuation of Amil-induced voltage deflections and Amil-sensitive transport ($I_{eq-Amil}$) after ATP stimulation. When CF primary cells were treated with DGK_{inh}, Amil-sensitive Na^+ absorption was largely reduced to its physiological levels (Figures 6B and 6C). Moreover, ATP-stimulation only slightly further reduced Na^+ absorption. Remarkably, in non-CF airway cultures, $I_{eq-Amil}$ was lower than in CF airways and DGK_{inh} showed no significant effects on ion transport. These results indicate that enhanced Amil-sensitive Na^+ absorption is attenuated by DGK_{inh} to levels found in normal non-CF airways, i.e., restoring Na^+ transport homeostasis but not completely blocking it. DGK inhibitors are therefore a potentially valuable tool for the treatment of CF lung disease. Notably DGK_{inh} also delayed transepithelial fluid absorption in human CF primary epithelial airway cells

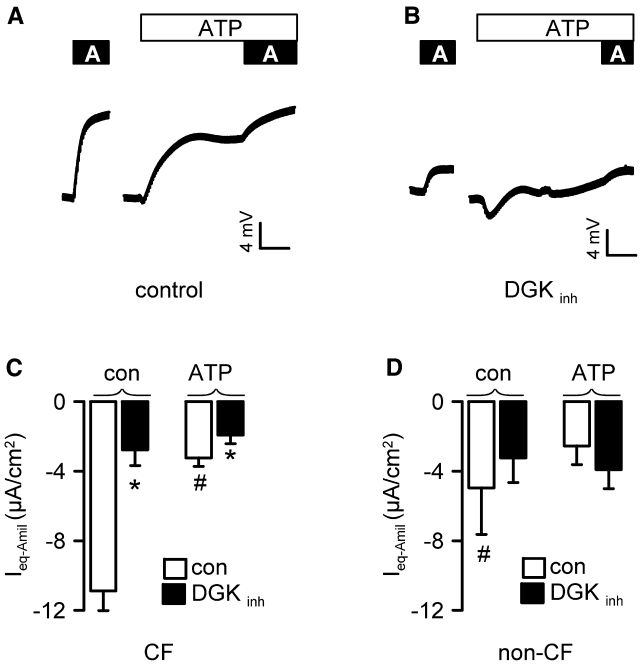

Figure 6. DGK and CNTFR Inhibit ENaC in Primary CF Airway Cultures

(A and B) Transepithelial voltages measured in primary CF bronchial epithelial cells grown in an air liquid interface (ALI) by Ussing chamber. (A) Effects of Amil (10 μM) and stimulation of apical P2Y receptors by ATP (100 μM); and (B) after incubation with 25 μM DGK_{inh} for 4–6 hr.

(C) Summary of Amil-sensitive transport ($I_{eq-Amil}$) before and after exposure to DGK_{inh} and inhibition of $I_{eq-Amil}$ by ATP in CF airways.

(D) Summary of $I_{eq-Amil}$ and effects of DGK_{inh} and ATP in non-CF airways.

Mean ± SEM; n = 5–7 for non-CF and CF patients, respectively. # indicates significantly different from control and CF, respectively ($p < 0.05$, unpaired t test). *indicates significant effect of Amil ($p < 0.05$, unpaired t test). See also Figure S7.

and again inhibition was more pronounced in CF versus non-CF cells (Figures S7A and S7B).

DISCUSSION

The aim of this study was to perform a loss-of-function screen mainly designed to globally identify regulators of ENaC traffic/function, with the ultimate goal of finding putative drug targets for CF. To this end, we used a high-content siRNA screen whose endpoint was a fluorescent cell-live microscopy assay measuring ENaC activity on an individual cell basis. Analysis of the primary screen data led to the identification of 1,626 ENaC regulators: 739 activator and 887 inhibitor genes. Submission of the primary hits to bioinformatic annotation showed the phosphatidylinositol (PI) signaling system as the most significantly enriched pathway, represented by 30 genes. Evidence of suppression by the siRNAs was previously shown (Neumann et al., 2010) by qRT-PCR tests for >97% of the tested transcripts (see Supplemental Information). Nonetheless, secondary validation of primary hits, i.e., confirmation with additional siRNAs, is vital.

Because our main goal was to find new ways of inhibiting ENaC, we focused the hit validation on genes activating ENaC. We thus selected the top ~60% (456) genes out of the 739 ENaC activators and on the 30 genes in the PI pathway. Whereas 160 genes were confirmed by at least two independent siRNAs as ENaC activators in the former group (~30%), 11 genes (37%) from the PI pathway could be validated: ten ENaC activators and one inhibitor. These validation percentages are within the range usually found in similar siRNA screens (Neumann et al., 2010; Simpson et al., 2012). However, this stringent validation does not completely rule out as ENaC regulators genes that in the primary screen had an effect but could not be confirmed by an independent siRNA. Indeed, other siRNAs acting at higher efficiency may also achieve the effect observed in the primary screen.

Next, we classified the validated hits in relation to the three major known pathways regulating ENaC. The obtained hit classification (Figure 3B and Dataset S4) may be used to generate multiple hypotheses in various types of analysis. For example, the genes whose siRNAs are sensitive to all three treatments (class II) are probably those responsible for the crosstalking among those three ENaC regulatory pathways. Indeed, the ubiquitination status of ENaC by Nedd4-2, for instance, was shown to affect the proteolytic cleavage of the channel (Ruffieux-Daidié et al., 2008), but the mechanism is still unknown. Accordingly, the nine genes in class VII (Figure 3B), i.e., whose siRNA no longer inhibit ENaC under aprotinin nor under Nedd4-2-siRNA, could be related to such crosstalk: *KCNQ3*, *TAS2R1*, *TNFRSF1B*, *B4GALT6*, *KIFAP3*, *CDK10*, *GRINA*, *SCGB3A1*, and *IFIH1* (Dataset S4). One of these (*SCGB3A1*) is downregulated in CF nasal epithelium (Clarke et al., 2013) and CF bronchial epithelium (Ogilvie et al., 2011) and upregulated during air-liquid interface differentiation of human bronchial epithelial cells (Ross et al., 2007).

Also of particular interest are the 11 validated hits (*ADAR*; *AKAP14*; *ARHGEF11*; *BRD4*; *DPP9*; *KIFAP3*; *MAST3*; *PIK3CA*; *RIPK2*; *RYK*; SCARB2), which no longer inhibited ENaC when WT-CFTR was expressed, but were insensitive to presence of F508del mutant (class IV*, Dataset S4). These genes deserve future examination to elucidate how WT-CFTR (but not F508del-CFTR) prevents the ENaC-mediated Na^+ hyperabsorption in non-CF individuals. Notably, 4 out of these 11 hits (AKAP14, KIFAP3, MAST3, and ARHGEF11) are cytoskeleton-related proteins and ARHGEF11 is a regulator of Rho, which we recently showed to be critical for the plasma membrane rescue of F508del-CFTR (Moniz et al., 2013). Interestingly, these four hits were also found to affect secretory traffic in a previous screen (Simpson et al., 2012).

Although these hit classes are of interest and deserve further examination, detailed investigation of all underlying mechanisms goes well beyond the present study. Nevertheless, we decided to focus on original ENaC activators outside the known pathways (i.e., hits in classes I and I*) as putative drug targets. Among the seven genes in these two classes (Dataset S4)—*ACY3*; *CCNI*; *CNTFR*; *DGKι*; *IQCF1*; *MEST*; and *SERPINB3*—we selected two for further mechanistic studies: *DGKι* as a putative drug target and *CNTFR* as a novel ENaC regulator.

Isoform iota of DGKι, never directly described as an ENaC modulator, was thus further investigated using different approaches, and results indicate that DGKι supports ENaC activity

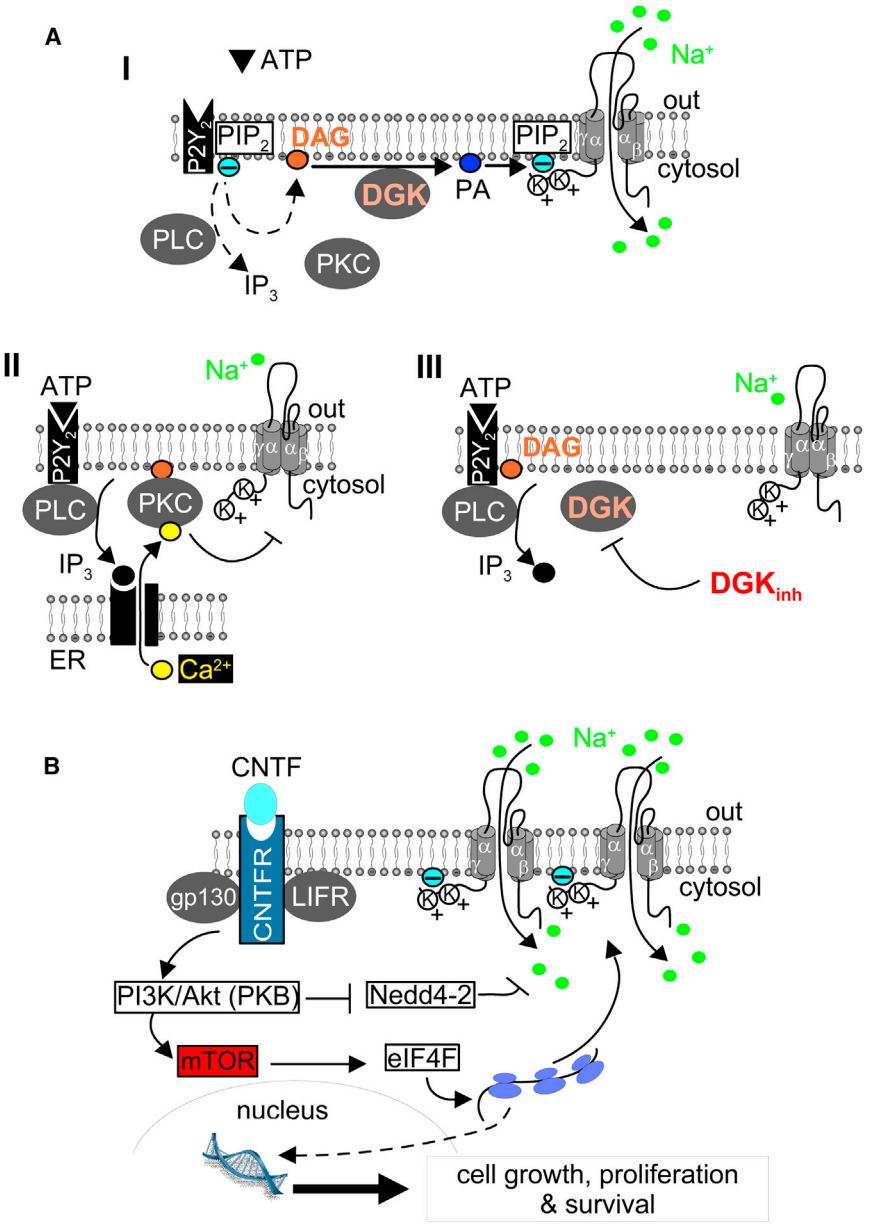

Figure 7. Role of DGK and CNTFR on ENaC Activation

(A) DGK maintains ENaC-activity by regenerating the PIP_2 in the inner leaflet of apical plasma membrane (I). Activation of P2Y receptors induces PIP_2 hydrolysis, thereby enhancing intracellular IP_3 and Ca^{2+}. ENaC is inhibited by PKC, which is activated by DAG and Ca^{2+}, and by lack of ENaC anchoring to PIP_2 via N-terminal lysines (II). Inhibition of DGK depletes the membrane of PIP_2, thus inhibiting ENaC (III).

(B) Binding of CNTF to CNTFR may activate multiple intracellular pathways, leading to suppression of Nedd4-2, which increases activity and membrane expression of ENaC (Koehl et al., 2010). mTOR upregulates the transcriptional elongation factor eIF4F, which is also in charge of postnatal upregulation of ENaC due to increase in O_2 partial pressure (Otulakowski et al., 2007).

by maintaining PIP_2 levels in the inner plasma membrane leaflet. Indeed, DGKι is a lipid cycle component that is essential for regeneration of phosphatidylinositols such as PIP_2 and our results support the concept that DGK activates ENaC by regenerating the PIP_2 pool present in the inner leaflet of the apical plasma membrane (Figure 7A). Negatively charged phosphoinositides like PIP_2 interact with positively charged lysine residues at the N terminus of β- and γ-ENaC, which is necessary to keep the channel open (Kunzelmann et al., 2005). ATP stimulation of purinergic receptors activates PLC and consequently PIP_2 hydrolysis, which leads to ENaC inhibition (Figure 7B). Here, we also showed that si-DGKι or its chemical inhibition, reduces ENaC activity to ~50% in various cell types and mouse trachea and down to ~65% in CF human primary airway cultures. Notably, attenuation of ENaC by DGK inhibition was pronounced in CF airway cultures but was not significant in non-CF airways. DGK inhibition also caused a delay in transepithelial fluid absorption in CF (but not in non-CF) human primary airway cultures. Importantly, DGKι inhibition in CF primary airway cells does not completely block ENaC activity. Instead, it restores Na^+-absorption to normal levels of non-CF airways, a condition that should be fulfilled for potential drugs modulating ENaC. These data demonstrate the physiological relevance of inhibiting DGKι to restore ENaC function, Na^+ homeostasis, and fluid absorption. As expression levels of DGKι in cultured cells parallel those in native human lung tissues (Figure S5), DGKι appears a physiologically relevant potential drug target for CF. When inhibiting DGK in cells even for long periods of time (up to 72 hr), we did not recognize any obvious toxicity. Moreover the exclusive localization of PIP_2 in the apical membrane (Bryant and Mostov, 2008; Gálvez-Santisteban et al., 2012) should limit the chance for unexpected effects of DGK inhibitors. Interestingly, this target has been recently proposed to treat inflammation, coagulation, and cancer (Holden et al., 2011; Marumo et al., 2012; Filigheddu et al., 2011) with no reported toxicity.

Taken together, inhibition of DGKι, an original regulator of ENaC activity, seems to constitute a powerful tool to normalize Na^+ absorption and fluid homeostasis in ASL of CF airways.

There is yet an ongoing controversy with respect to Na^+ hyperabsorption as the cause of CF lung disease, particularly in light of more recent studies on newborn CF pigs, which cast serious doubt on the concept of hyperabsorption (Chen et al., 2010). However, studies on human native airways (Boucher et al.,

1988; Mall et al., 1998) and ENaC-overexpressing mice (Mall et al., 2004) still clearly support this concept (recently reviewed in Kunzelmann and Schreiber, 2012). Despite this controversy, inhibition of ENaC has been demonstrated in multiple studies to enhance ASL and to improve mucociliary clearance. Treatment with hypertonic saline, shown to cause ENaC inhibition, has also been demonstrated to improve mucus clearance and lung function (Donaldson et al., 2006).

Another significant hit in the present screen, CNTFR, with no known role in ENaC regulation, was selected to demonstrate the screen's potential to identify unexpected ENaC regulators, and indeed, it was proven to regulate ENaC. Although data here do not fully explore the intracellular pathways leading to ENaC activation through CNTFR, they strongly suggest that CNTFR operates through the mTOR pathway. In fact, earlier studies in mice with enhanced mTOR activity caused by reduced expression of the tumor suppressor APC, demonstrated pronounced upregulation of ENaC (Ousingsawat et al., 2008). This is probably due to upregulation of the transcriptional elongation factor eIF4F, which is also in charge of postnatal ENaC upregulation (Otulakowski et al., 2007).

Taken together, the present results demonstrate the power of microscopy siRNA screens in discovering novel regulators of ion channels and drug targets. Detailed studies on two screen hits regulating ENaC—DGKι and CNTFR—clearly led to original pathways. Importantly, DGKι seems well-suited as a potential novel drug target for CF because by its inhibition ENaC activity is reduced, and both Na^+ and fluid absorption are normalized in CF airways to non-CF levels.

EXPERIMENTAL PROCEDURES

Materials

The FMP/Amil live-cell assay was previously described (Almaça et al., 2011). The siRNAs (n = 17,840) targeting 6,409 different genes (Dataset S1) came from three chemically synthesized libraries: the druggable (Ambion), the kinome (Ambion), and the secretome library (Quiagen), as described (Simpson et al., 2012). Additional reagents are in Supplemental Information.

Cell Culture

Human alveolar type II epithelial A549 cells (ATCC, Cat no. CCL-185) were grown with or without dexamethasone (Dexa) as before, as well as WT- or F508del-CFTR transduced A549 cells (Almaça et al., 2011). More cell culture details are in Supplemental Information.

FMP/Amiloride Assay

The live-cell assay used to identify novel regulators of ENaC activity was performed with the voltage-sensitive dye FMP and 30 μM Amil, as described (Almaça et al., 2011) on A549 cells reverse-transfected for 48 hr with different siRNAs (Erfle et al., 2007).

Automated Microscopy and High-Content siRNA Screening

Cells (~150,000 cells) were plated in 1.5 ml of culture medium in siRNA prespotted chambered slides. After 48 hr, cells were incubated for 10 min with FMP as described (Almaça et al., 2011). Cells on siRNA spots (1-384) were imaged with 10× objective in Cy3 channel, the FMP solution was then automatically replaced by FMP/Amil; after 3 min, the same image acquisition routine started.

Secondary/Validation Screen and Hit Classification into ENaC Pathways

For validation of primary screen hits, we used one to two additional independent siRNAs targeting the top 456 hit genes (targeted by ENaC-inhibiting siRNAs) and performed the same FMP/Amil assay, image quantification, and data analysis as for the primary screen, but with a different normalization (see Supplemental Information). In order to classify the hits into three well-known ENaC pathways, namely activation by proteolytic cleavage; Nedd4-2-mediated internalization and degradation; and CFTR inhibition, parental A549 cells were submitted to the different treatments detailed in Supplemental Information.

Image Quantification and Primary Screen Data Analysis

For each acquired image the FMP-fluorescence intensity was measured before and after Amil addition using a customized LabView-based program. Complete details are in Supplemental Information.

Bioinformatic Analysis

The 1,657 primary screen hits (Dataset S1) were submitted to DAVID bioinformatic analysis to identify the biological pathways (from the KEGG database) most significantly overrepresented (Huang et al., 2009). For GO analysis of validated genes, we used AmiGO (Carbon et al., 2009). Pathway analysis of the validated screen hits was performed using ENSEMBL IDs (version 61) on "BioCompendium." Bioinformatic analysis details are in Supplemental Information.

Ussing Chamber Experiments

Non-CF and CF primary human bronchial epithelial cells, cultured as described (Supplemental Information), polarized monolayers of H441 or M1 cells were grown on permeable supports (Millipore) for 10 days and then mounted into a perfused micro-Ussing chamber with continuous (luminal and basolateral) perfusion at 5–10 ml/min. Tracheal tissue was isolated from mice. Experiments were carried out under open-circuit conditions at 37°C. Details are in Supplemental Information.

Target Validation by Double-Electrode Voltage-Clamp

Xenopus oocytes were injected with cRNA (10 ng, 47 nl double-distilled water) encoding wild-type $\alpha\beta\gamma$-ENaC subunits, α-ENaC with a C terminus truncation (α_{H648X}), and β-ENaC with N terminus deletion ($\beta_{\Delta N}$). Water injected oocytes served as controls. Two to three days after injection, oocytes were impaled with two electrodes as previously described (Kunzelmann et al., 2005). Unpaired Student's t test or ANOVA were used for statistical analysis, as indicated, and p values lower than 0.05 were accepted as significant.

Plate Reader Experiments

To characterize the mechanism underlying ENaC regulation by DGK, the FMP/Amil assay was performed on A549 cells using a plate reader (Novostar). A549 cells were transfected with either a scrambled or DGKι-siRNA for 72 hr and the activity of several enzymes involved in phospholipid metabolism and signaling was modulated with specific inhibitors and/or activators (for 2–5 hr)—PLC activator m3M3FBS at 25 μM, PLC inhibitor U73122 at 5 μM, PI3K inhibitor LY294002 at 50 nM, PKC activator PMA at 100 nM, PKC inhibitor BIM at 50 nM.

SUPPLEMENTAL INFORMATION

Supplemental Information includes Extended Experimental Procedures, seven figures, and five datasets and can be found with this article online at http://dx.doi.org/10.1016/j.cell.2013.08.045.

ACKNOWLEDGMENTS

This work was supported by EU-grant TargetScreen2 (LSH-2005-1.2.5-3-037365), strategic grant PEst-OE/BIA/UI4046/2011 (BioFIG), and FCT/POCTI-PTDC/SAU-GMG/122299/2010; DFG SFB699 A6; Vs. 28.12.2010. J.A., D.F., M.S., and I.U. were recipients of PhD fellowships SFRH/BD/29134/2006, SFRH/BD/43313/2008, SFRH/BD/35936/2007, and SFRH/BD/69180/2010, respectively, from FCT, Portugal. We acknowledge the scientific support of Drs. Beate Neumann and Thomas Walter as well as the expert technical assistance by Miriam Reiss, Jutta Bulkescher, Brigitte

Joggerst-Thomalla, Marta Palma, Tze Heng, and Volker Hilsenstein, assistance with with microscope programming by Siegfrid Winkler, and data analysis by the electronic workshop from EMBL, Heidelberg. The authors are grateful to Professor J. Fragata and his team at the Cardio-Thoracic Surgery Department of the Hospital de Santa Marta (Lisboa) for access to explanted lungs from CF patients, to Professor Jens Leipziger (Aarhus University, Denmark) for critically revising the manuscript, and to Dr. Michael Gray (Newcastle University, UK) for comments. R.P., K.K., and M.D.A. designed the study; J.A., D.F., M.S., I.U., L.S., L.A.C., J.P.M., and M.S. performed experiments and generated data; J.A., D.F., M.S., I.U., L.S., L.A.C., J.-K.H., C.C., W.H., and R.S. analyzed data; L.A.C., C.C., R.S., R.P., K.K., and M.D.A. interpreted data; J.A., K.K., and M.D.A. wrote the article; R.P., K.K., and M.D.A. revised the article; R.P., K.K., and M.D.A. obtained funding. All authors approved the final manuscript.

Received: March 3, 2012
Revised: July 8, 2013
Accepted: August 26, 2013
Published: September 12, 2013

REFERENCES

Almaça, J., Dahimène, S., Appel, N., Conrad, C., Kunzelmann, K., Pepperkok, R., and Amaral, M.D. (2011). Functional genomics assays to study CFTR traffic and ENaC function. Methods Mol. Biol. *742*, 249–264.

Althaus, M., Clauss, W.G., and Fronius, M. (2011). Amiloride-sensitive sodium channels and pulmonary edema. Pulm. Med. *2011*, 830320.

Amaral, M.D., and Kunzelmann, K. (2007). Molecular targeting of CFTR as a therapeutic approach to cystic fibrosis. Trends Pharmacol. Sci. *28*, 334–341.

Berthiaume, Y., and Matthay, M.A. (2007). Alveolar edema fluid clearance and acute lung injury. Respir. Physiol. Neurobiol. *159*, 350–359.

Bonny, O., and Hummler, E. (2000). Dysfunction of epithelial sodium transport: from human to mouse. Kidney Int. *57*, 1313–1318.

Boucher, R.C. (2007). Cystic fibrosis: a disease of vulnerability to airway surface dehydration. Trends Mol. Med. *13*, 231–240.

Boucher, R.C., Cotton, C.U., Gatzy, J.T., Knowles, M.R., and Yankaskas, J.R. (1988). Evidence for reduced Cl^- and increased Na^+ permeability in cystic fibrosis human primary cell cultures. J. Physiol. *405*, 77–103.

Bryant, D.M., and Mostov, K.E. (2008). From cells to organs: building polarized tissue. Nat. Rev. Mol. Cell Biol. *9*, 887–901.

Butterworth, M.B., Edinger, R.S., Frizzell, R.A., and Johnson, J.P. (2009). Regulation of the epithelial sodium channel by membrane trafficking. Am. J. Physiol. Renal Physiol. *296*, F10–F24.

Canessa, C.M., Schild, L., Buell, G., Thorens, B., Gautschi, I., Horisberger, J.D., and Rossier, B.C. (1994). Amiloride-sensitive epithelial Na^+ channel is made of three homologous subunits. Nature *367*, 463–467.

Carbon, S., Ireland, A., Mungall, C.J., Shu, S., Marshall, B., and Lewis, S.; AmiGO Hub; Web Presence Working Group. (2009). AmiGO: online access to ontology and annotation data. Bioinformatics *25*, 288–289.

Chen, J.H., Stoltz, D.A., Karp, P.H., Ernst, S.E., Pezzulo, A.A., Moninger, T.O., Rector, M.V., Reznikov, L.R., Launspach, J.L., Chaloner, K., et al. (2010). Loss of anion transport without increased sodium absorption characterizes newborn porcine cystic fibrosis airway epithelia. Cell *143*, 911–923.

Chung, N., Zhang, X.D., Kreamer, A., Locco, L., Kuan, P.F., Bartz, S., Linsley, P.S., Ferrer, M., and Strulovici, B. (2008). Median absolute deviation to improve hit selection for genome-scale RNAi screens. J. Biomol. Screen. *13*, 149–158.

Clarke, L.A., Sousa, L., Barreto, C., and Amaral, M.D. (2013). Changes in transcriptome of native nasal epithelium expressing F508del-CFTR and intersecting data from comparable studies. Respir. Res. *14*, 38.

Clunes, L.A., Davies, C.M., Coakley, R.D., Aleksandrov, A.A., Henderson, A.G., Zeman, K.L., Worthington, E.N., Gentzsch, M., Kreda, S.M., Cholon, D., et al. (2012). Cigarette smoke exposure induces CFTR internalization and insolubility, leading to airway surface liquid dehydration. FASEB J. *26*, 533–545.

Debonneville, C., Flores, S.Y., Kamynina, E., Plant, P.J., Tauxe, C., Thomas, M.A., Münster, C., Chraïbi, A., Pratt, J.H., Horisberger, J.D., et al. (2001). Phosphorylation of Nedd4-2 by Sgk1 regulates epithelial Na^+ channel cell surface expression. EMBO J. *20*, 7052–7059.

Donaldson, S.H., and Boucher, R.C. (2007). Sodium channels and cystic fibrosis. Chest *132*, 1631–1636.

Donaldson, S.H., Bennett, W.D., Zeman, K.L., Knowles, M.R., Tarran, R., and Boucher, R.C. (2006). Mucus clearance and lung function in cystic fibrosis with hypertonic saline. N. Engl. J. Med. *354*, 241–250.

Erfle, H., Neumann, B., Liebel, U., Rogers, P., Held, M., Walter, T., Ellenberg, J., and Pepperkok, R. (2007). Reverse transfection on cell arrays for high content screening microscopy. Nat. Protoc. *2*, 392–399.

Filigheddu, N., Sampietro, S., Chianale, F., Porporato, P.E., Gaggianesi, M., Gregnanin, I., Rainero, E., Ferrara, M., Perego, B., Riboni, F., et al. (2011). Diacylglycerol kinase α mediates 17-β-estradiol-induced proliferation, motility, and anchorage-independent growth of Hec-1A endometrial cancer cell line through the G protein-coupled estrogen receptor GPR30. Cell. Signal. *23*, 1988–1996.

Gaillard, E.A., Kota, P., Gentzsch, M., Dokholyan, N.V., Stutts, M.J., and Tarran, R. (2010). Regulation of the epithelial Na^+ channel and airway surface liquid volume by serine proteases. Pflugers Arch. *460*, 1–17.

Gálvez-Santisteban, M., Rodriguez-Fraticelli, A.E., Bryant, D.M., Vergarajauregui, S., Yasuda, T., Bañón-Rodríguez, I., Bernascone, I., Datta, A., Spivak, N., Young, K., et al. (2012). Synaptotagmin-like proteins control the formation of a single apical membrane domain in epithelial cells. Nat. Cell Biol. *14*, 838–849.

Gentzsch, M., Dang, H., Dang, Y., Garcia-Caballero, A., Suchindran, H., Boucher, R.C., and Stutts, M.J. (2010). The cystic fibrosis transmembrane conductance regulator impedes proteolytic stimulation of the epithelial Na^+ channel. J. Biol. Chem. *285*, 32227–32232.

Hirsh, A.J., Molino, B.F., Zhang, J., Astakhova, N., Geiss, W.B., Sargent, B.J., Swenson, B.D., Usyatinsky, A., Wyle, M.J., Boucher, R.C., et al. (2006). Design, synthesis, and structure-activity relationships of novel 2-substituted pyrazinoylguanidine epithelial sodium channel blockers: drugs for cystic fibrosis and chronic bronchitis. J. Med. Chem. *49*, 4098–4115.

Holden, N.J., Savage, C.O., Young, S.P., Wakelam, M.J., Harper, L., and Williams, J.M. (2011). A dual role for diacylglycerol kinase generated phosphatidic acid in autoantibody-induced neutrophil exocytosis. Mol. Med. *17*, 1242–1252.

Huang, W., Sherman, B.T., and Lempicki, R.A. (2009). Systematic and integrative analysis of large gene lists using DAVID bioinformatics resources. Nat. Protoc. *4*, 44–57.

Itani, O.A., Auerbach, S.D., Husted, R.F., Volk, K.A., Ageloff, S., Knepper, M.A., Stokes, J.B., and Thomas, C.P. (2002). Glucocorticoid-stimulated lung epithelial Na^+ transport is associated with regulated ENaC and sgk1 expression. Am. J. Physiol. Lung Cell. Mol. Physiol. *282*, L631–L641.

Ji, H.L., Su, X.F., Kedar, S., Li, J., Barbry, P., Smith, P.R., Matalon, S., and Benos, D.J. (2006). Delta-subunit confers novel biophysical features to alpha beta gamma-human epithelial sodium channel (ENaC) via a physical interaction. J. Biol. Chem. *281*, 8233–8241.

Kimura, T., Kawabe, H., Jiang, C., Zhang, W., Xiang, Y.Y., Lu, C., Salter, M.W., Brose, N., Lu, W.Y., and Rotin, D. (2011). Deletion of the ubiquitin ligase Nedd4L in lung epithelia causes cystic fibrosis-like disease. Proc. Natl. Acad. Sci. USA *108*, 3216–3221.

Knowles, M.R., Church, N.L., Waltner, W.E., Yankaskas, J.R., Gilligan, P., King, M., Edwards, L.J., Helms, R.W., and Boucher, R.C. (1990). A pilot study of aerosolized amiloride for the treatment of lung disease in cystic fibrosis. N. Engl. J. Med. *322*, 1189–1194.

Koehl, G.E., Spitzner, M., Ousingsawat, J., Schreiber, R., Geissler, E.K., and Kunzelmann, K. (2010). Rapamycin inhibits oncogenic intestinal ion channels and neoplasia in $APC^{(Min/+)}$ mice. Oncogene *29*, 1553–1560.

Kunzelmann, K., and Schreiber, R. (2012). Airway epithelial cells—hyperabsorption in CF? Int. J. Biochem. Cell Biol. *44*, 1232–1235.

Kunzelmann, K., Kathöfer, S., and Greger, R. (1995). Na+ and Cl- conductances in airway epithelial cells: increased Na^+ conductance in cystic fibrosis. Pflugers Arch. *431*, 1–9.

Kunzelmann, K., Bachhuber, T., Regeer, R., Markovich, D., Sun, J., and Schreiber, R. (2005). Purinergic inhibition of the epithelial Na^+ transport via hydrolysis of PIP_2. FASEB J. *19*, 142–143.

Lifton, R.P., Gharavi, A.G., and Geller, D.S. (2001). Molecular mechanisms of human hypertension. Cell *104*, 545–556.

Lu, M., Wang, J., Jones, K.T., Ives, H.E., Feldman, M.E., Yao, L.J., Shokat, K.M., Ashrafi, K., and Pearce, D. (2010). mTOR complex-2 activates ENaC by phosphorylating SGK1. J. Am. Soc. Nephrol. *21*, 811–818.

Mall, M., Bleich, M., Greger, R., Schreiber, R., and Kunzelmann, K. (1998). The amiloride-inhibitable Na^+ conductance is reduced by the cystic fibrosis transmembrane conductance regulator in normal but not in cystic fibrosis airways. J. Clin. Invest. *102*, 15–21.

Mall, M., Grubb, B.R., Harkema, J.R., O'Neal, W.K., and Boucher, R.C. (2004). Increased airway epithelial Na^+ absorption produces cystic fibrosis-like lung disease in mice. Nat. Med. *10*, 487–493.

Marumo, M., Nakano, T., Takeda, Y., Goto, K., and Wakabayashi, I. (2012). Inhibition of thrombin-induced Ca^{2+} influx in platelets by R59949, an inhibitor of diacylglycerol kinase. J. Pharm. Pharmacol. *64*, 855–861.

Moniz, S., Sousa, M., Moraes, B., Mendes, A.I., Palma, M., Barreto, C., Fragata, J.I., Amaral, M.D., and Matos, P. (2013). HGF stimulation of Rac1 signaling enhances pharmacological correction of the most prevalent cystic fibrosis mutant F508del-CFTR. ACS Chem. Biol. *8*, 432–442.

Neumann, B., Walter, T., Hériché, J.K., Bulkescher, J., Erfle, H., Conrad, C., Rogers, P., Poser, I., Held, M., Liebel, U., et al. (2010). Phenotypic profiling of the human genome by time-lapse microscopy reveals cell division genes. Nature *464*, 721–727.

O'Brodovich, H. (1991). Epithelial ion transport in the fetal and perinatal lung. Am. J. Physiol. *261*, C555–C564.

Ogilvie, V., Passmore, M., Hyndman, L., Jones, L., Stevenson, B., Wilson, A., Davidson, H., Kitchen, R.R., Gray, R.D., Shah, P., et al. (2011). Differential global gene expression in cystic fibrosis nasal and bronchial epithelium. Genomics *98*, 327–336.

Otulakowski, G., Duan, W., Gandhi, S., and O'brodovich, H. (2007). Steroid and oxygen effects on eIF4F complex, mTOR, and ENaC translation in fetal lung epithelia. Am. J. Respir. Cell Mol. Biol. *37*, 457–466.

Ousingsawat, J., Spitzner, M., Schreiber, R., and Kunzelmann, K. (2008). Upregulation of colonic ion channels in APC $^{(\ Min/+\ )}$ mice. Pflugers Arch. *456*, 847–855.

Pochynyuk, O., Tong, Q., Medina, J., Vandewalle, A., Staruschenko, A., Bugaj, V., and Stockand, J.D. (2007). Molecular determinants of $PI(4,5)P_2$ and $PI(3,4,5)P_3$ regulation of the epithelial Na^+ channel. J. Gen. Physiol. *130*, 399–413.

Pochynyuk, O., Bugaj, V., and Stockand, J.D. (2008). Physiologic regulation of the epithelial sodium channel by phosphatidylinositides. Curr. Opin. Nephrol. Hypertens. *17*, 533–540.

Riordan, J.R. (2008). CFTR function and prospects for therapy. Annu. Rev. Biochem. *77*, 701–726.

Ritzerfeld, J., Remmele, S., Wang, T., Temmerman, K., Brügger, B., Wegehingel, S., Tournaviti, S., Strating, J.R., Wieland, F.T., Neumann, B., et al. (2011). Phenotypic profiling of the human genome reveals gene products involved in plasma membrane targeting of SRC kinases. Genome Res. *21*, 1955–1968.

Ross, A.J., Dailey, L.A., Brighton, L.E., and Devlin, R.B. (2007). Transcriptional profiling of mucociliary differentiation in human airway epithelial cells. Am. J. Respir. Cell Mol. Biol. *37*, 169–185.

Ruffieux-Daidié, D., Poirot, O., Boulkroun, S., Verrey, F., Kellenberger, S., and Staub, O. (2008). Deubiquitylation regulates activation and proteolytic cleavage of ENaC. J. Am. Soc. Nephrol. *19*, 2170–2180.

Simpson, J.C., Joggerst, B., Laketa, V., Verissimo, F., Cetin, C., Erfle, H., Bexiga, M.G., Singan, V.R., Hériché, J.K., Neumann, B., et al. (2012). Genome-wide RNAi screening identifies human proteins with a regulatory function in the early secretory pathway. Nat. Cell Biol. *14*, 764–774.

Snouwaert, J.N., Brigman, K.K., Latour, A.M., Malouf, N.N., Boucher, R.C., Smithies, O., and Koller, B.H. (1992). An animal model for cystic fibrosis made by gene targeting. Science *257*, 1083–1088.

Staub, O., Gautschi, I., Ishikawa, T., Breitschopf, K., Ciechanover, A., Schild, L., and Rotin, D. (1997). Regulation of stability and function of the epithelial Na^+ channel (ENaC) by ubiquitination. EMBO J. *16*, 6325–6336.

Stockand, J.D., Bao, H.F., Schenck, J., Malik, B., Middleton, P., Schlanger, L.E., and Eaton, D.C. (2000). Differential effects of protein kinase C on the levels of epithelial Na^+ channel subunit proteins. J. Biol. Chem. *275*, 25760–25765.

Wang, X., Venable, J., LaPointe, P., Hutt, D.M., Koulov, A.V., Coppinger, J., Gurkan, C., Kellner, W., Matteson, J., Plutner, H., et al. (2006). Hsp90 cochaperone Aha1 downregulation rescues misfolding of CFTR in cystic fibrosis. Cell *127*, 803–815.

Yokogami, K., Wakisaka, S., Avruch, J., and Reeves, S.A. (2000). Serine phosphorylation and maximal activation of STAT3 during CNTF signaling is mediated by the rapamycin target mTOR. Curr. Biol. *10*, 47–50.

Yue, G., Malik, B., Yue, G., and Eaton, D.C. (2002). Phosphatidylinositol 4,5-bisphosphate (PIP_2) stimulates epithelial sodium channel activity in A6 cells. J. Biol. Chem. *277*, 11965–11969.